2018-01-01

Investigation of flocculation dynamics under changing hydrodynamic forcing on an intertidal mudflat

Guo, C

10.1016/j.margeo.2017.10.001
Marine Geology
Elsevier

Marine Geology 395 (2018) 120–132

Contents lists available at ScienceDirect

Marine Geology

journal homepage: www.elsevier.com/locate/margo

Investigation of flocculation dynamics under changing hydrodynamic forcing on an intertidal mudflat

Chao Guo[a], Qing He[a,*], Bram C. van Prooijen[b], Leicheng Guo[a], Andrew J. Manning[c,d,e], Sarah Bass[c]

[a] State Key Laboratory of Estuarine and Coastal Research, East China Normal University, Shanghai 200062, People's Republic of China
[b] Section of Environmental Fluid Mechanics, Faculty of Civil Engineering and Geosciences, Delft University of Technology, PO Box 5048, 2600, GA, Delft, The Netherlands
[c] School of Marine Science and Engineering, University of Plymouth, Drake Circus, Plymouth, Devon PL4 8AA, United Kingdom
[d] HR Wallingford, Howbery Park, Wallingford OX10 8BA, United Kingdom
[e] Department of Geography, Environment and Earth Sciences, University of Hull, Hull HU6 7RX, United Kingdom

ARTICLE INFO

Keywords:
Flocculation
Floc effective density
Erosion and deposition
Tidal flat
Storm
The Scheldt estuary

ABSTRACT

In situ floc size and turbulent shear stress were measured together with suspended sediment concentration to investigate the floc properties under changing hydrodynamic forcing over the intertidal mudflat. A tripod system was established in the field for a period of approximately one month, including ~6 days of stormy conditions in the middle of the investigation period. Mean floc size exhibited strong temporal variations within a tidal cycle, and inverse relationship was found between mean floc size and shear stress. Suspended sediment concentration (SSC) can modulate the flocculation dynamics when shear stress decreases down to enhancing flocculation. Asymmetrical behaviors of floc sizes between flood and ebb phases were identified, with overall larger floc sizes in flood than in ebb tide under the same shear stresses. Floc structure showed different properties under calm and stormy conditions, and the variable fractal dimension and variable primary particle size were more convincing in simulating the variation of floc effective density with mean floc size during the storm period, which was inferred to be related to the resuspension of bed sediment as well as organic matter. A total of 110 mm bed erosion was measured during the storm, and erosion events occurred only around low water, due to the high current-wave combined bed shear stress and off-shore current. After the storm, ~40% of the erosion recovered within one week, and the fast settling of large flocs around high water plays significant role in the deposition process, leading to ~60% of the recovery.

1. Introduction

Intertidal mudflats provide a transition zone and protective barrier between land and estuary, and they have valuable functions in terms of ecosystem development (Dyer, 1998). The overall development of a mudflat depends on the relative balance between hydrodynamics (erosion) and sediment supply (sedimentation). On a short time-scale (i.e. the tidal cycle and spring-neap cycle), hydrodynamics dominated by tidal currents and waves determine the variations of suspended sediment flux and bed level. Sedimentation usually happens during relatively calm conditions due to settling and tidal asymmetry when the sediment supply is large (Christie and Dyer, 1998; Andersen and Pejrup, 2001; Deloffre et al., 2006). Episodic energetic events like storms are important for tidal flat development and can cause significant erosion within just a few tidal cycles (Christie et al., 1999; Andersen and Pejrup, 2001). On a seasonal time-scale, the importance of biological characteristics in modifying the initial erosion of the surface layer on a mudflat has also been found (e.g. Andersen, 2001; Uncles et al., 2003).

The transport of cohesive sediment is more complicated than non-cohesive sediment in particular due to flocculation, which is the result of simultaneously aggregation and floc break up processes (Winterwerp and Van Kesteren, 2004). Flocculation has been widely observed in varying fresh (e.g. river, lake), brackish (e.g. estuary, river deltas), and marine (e.g. open sea) waters (Droppo and Ongley, 1994; Fennessy et al., 1994; Manning and Dyer, 2007; Guo and He, 2011; Fettweis et al., 2014). Controls on flocculation processes are numerous and complex, including a number of physical and biochemical factors such as: the turbulent intensity, suspended sediment concentration (SSC), differential settling of particles, composition of primary particles, salinity, and content of organic matter and polymers, etc. (see e.g. Milligan and Hill, 1998; Manning and Dyer, 1999; Fugate and Friedrichs, 2003; Mietta et al., 2009; Verney et al., 2009; Sahin, 2014, among others).

* Corresponding author.
E-mail address: qinghe@sklec.ecnu.edu.cn (Q. He).

http://dx.doi.org/10.1016/j.margeo.2017.10.001
Received 1 May 2017; Received in revised form 24 September 2017; Accepted 3 October 2017
Available online 03 October 2017
0025-3227/

The conceptual diagram proposed by Dyer (1989) established that at low concentrations mean floc size first increases with shear stress at low values, followed by a decrease due to floc break up as shear stress increases, and at higher concentrations flocs are larger but more easily to be disrupted by shearing. This conceptual model was confirmed by a number of laboratory experiments and field measurements (e.g. Manning and Dyer, 1999; Kumar et al., 2010; Sahin, 2014). However, Winterwerp (1998) suggested that the long residence time of flocs required to achieve the equilibrium at low shear stress conditions ($\sim$2–3 s^{-1}) could explain the increase of floc size with shear rate. In the flocculation experiments using kaolinite, Mietta et al. (2009) found that when the shear rate was $< 35\ s^{-1}$, flocs became smaller with shear rate decreased as deposition prevented flocs from reaching the equilibrium. Moreover, in the laboratory experiments of Milligan and Hill (1998) and field survey of Xia et al. (2004) in a microtidal estuary, they found the influence of SSC on flocculation is minor. The inconsistency in these studies may be caused by varying constitutions of flocs and environmental conditions, therefore further studies in different estuarine systems with varied hydrodynamic forcing are required to extend our knowledge of flocculation dynamics.

Investigations on mudflats have shown that sediment deposition is predominantly in the form of flocs and that the fraction of flocs decreases with the increase of bed elevation at tidal scale (e.g. Christiansen et al., 2000; Voulgaris and Meyers, 2004; Hill et al., 2013; Law et al., 2013). The settling velocity of aggregated flocs is likely orders of magnitude larger than the settling of the primary particles. Flocculation therefore leads to an increased settling flux of mud to the bed (Soulsby et al., 2013; Mehta et al., 2014) and is particularly important to the mudflat deposition (Kranck and Milligan, 1992; Manning and Dyer, 2007). Higher turbulence levels tend to resuspend sediment from the bed and disrupt flocs, while as the tidal currents approach high or low water slack, large SSC combined with low turbulent intensities encourage the aggregation of flocs and result in rapid settling (Christie et al., 1999; Milligan et al., 2007). As the effective density of a floc tends to decrease with size due to increasing water content (Fennessy et al., 1994), floc settling velocity is controlled by both floc size and structure. However, variations of floc size as well as structure over a mudflat are still partially known as both hydrodynamic forcing and SSC can be highly variable around the low water environment, especially under episodic events like storms.

Given the many uncertainties as well as partially known aspects of floc dynamics on intertidal flats, a field campaign was set up. This paper is based on the results of in situ observations of floc properties and hydrodynamics on a mudflat covering continuous stormy and calm weather conditions. We aim to further explore the time-variant floc size and structure under different forcing conditions and how these contribute to the deposition of sediment on the mudflat.

2. Methodology

2.1. Site description

Fieldwork was conducted on the Kapellebank tidal flat, located in the lower part of the Westerschelde (Scheldt) Estuary in the Netherlands (Fig. 1a). The Scheldt estuary is a semidiurnal meso- to macro-tidal regime and extends 160 km in length. The mean tidal range at the estuary mouth fluctuates between 4.2 and 3.1 m during spring and neap tides, respectively. It increases up to about 6 m at a distance of 95 km landward, then gradually decreases to about 2.3 m. The mean SSC value in the lower Scheldt estuary (from the mouth to 58 km landward) is about 50 $mg\ l^{-1}$, and the main turbidity maximum zone (TMZ) locates at roughly 60 to 100 km from the mouth, mean SSC in the TMZ can reach 200 $mg\ l^{-1}$ (Chen et al., 2005a). The study site Kapellebank is a semi-enclosed flat at the channel outer-bend (Fig. 1b). It is about 35 km from the mouth, where the mean tidal range is $\sim$4.5 m, and this area is classified as well-mixed. Bed sediment on the Kapellebank is predominantly mud with a median grain size < 50 μm (Kuijper et al., 2004). The geometry of the tidal flat has a triangular shape with a length and width of approximately 1.8 and 0.8 km, respectively. The highest elevation of this tidal flat is about 0.6 m above the Normal Amsterdam Peil (NAP, which is approximately mean sea level). Bed level decreases towards the channel with a mild bed slope of about 3‰ (Fig. 1c). The observation site has an elevation of about -1.8 m and is approximately at the interface between intertidal and subtidal flats.

2.2. Field measurements

Field observations were conducted in 2014, between April 28 and May 22. The time-series were interrupted twice, i.e., May 2–3 and May 13–15, when instrument batteries were exchanged. A storm occurred between the 6th and 12th of May with the maximum wind speed reached 18 $m\ s^{-1}$ at the meteorological station Vlissingen, which is on the west side of the Kapellebank (Fig. 1b). Instruments were mounted on a frame constructed with stainless steel pipes and hammered at least 1.5 m into the bed to reduce horizontal and vertical vibrations.

Near-bed 3D current velocities were measured with a 6-MHz downward-looking acoustic Doppler velocimeter (ADV, Nortek Vector) with the sampling volume (2.65 cm^3) at 15 cm above the bed (cmab). ADV collected data at a sampling rate of 8 Hz continuously for 90 s, with a time interval between bursts of 10 min. Bed level variation was also measured by the ADV through recording the vertical distance between the acoustic transmitter and the bed surface with a resolution of 0.1 mm and an accuracy of ± 1 mm. Turbidity at 15 cmab was measured by an Optical Back-Scatter (OBS) 3 + sensor, which was logged by the ADV on one of its analogue channels. Wave climate at the study site was measured by a wave logger (OSSI-010-003C, Ocean Sensor Systems), which collected 4096 data points in 20 min bursts at a sampling rate of 10 Hz.

In situ floc size distributions were measured by a laser in situ scattering and transmissometry (LISST-100X, type C) instrument with the particle size spectra range between 2.5 and 500 μm. The instrument emits laser light through a sample volume of water, then it records the energy of scattered laser and inverts it into particle size distributions based on volume concentrations at 32 logarithmically spaced ring detectors, and each detector corresponds to one size range (Agrawal and Pottsmith, 2000). Laboratory and field evaluations by Gartner et al. (2001) demonstrated that the LISST is capable of determining particle size to within $\sim$10% with increasing error as particle size increases. Numerous articles have confirmed that LISST worked reasonably well over a range of environmental conditions (e.g. Mikkelsen and Pejrup, 2001; Guo and He, 2011; Safak et al., 2013; Ramírez -Mendoza et al., 2016). The work of Chen et al. (2005b) on a mud tidal flat $\sim$30 km downstream from our study site with a camera showed that the largest floc size was 290 ± 170 μm, indicating that the major portion of flocs in this area can be detected by the LISST-100C. The LISST was placed at 15 cmab with a sampling period of 3 min, and a 50% path reduction module was deployed to increase its sensitivity in turbid waters. For each sample period, 10 volume concentration distributions were collected over 30 s, and the averaged result was used to reduce short-time variations (Mikkelsen and Pejrup, 2001).

2.3. Data processing

2.3.1. Hydrodynamics

Commonly there are four methods to estimate shear stress: (1) Log Profile (LP) method, (2) Reynolds stress technique, (3) Turbulent Kinetic Energy (TKE) approach, and (4) energy dissipation measurement. The TKE approach was concluded as the most consistent one (Kim et al., 2000), and it best suited to this investigation with the presence of waves because the instantaneous velocity measurements from the ADV could provide both turbulent and wave characteristics

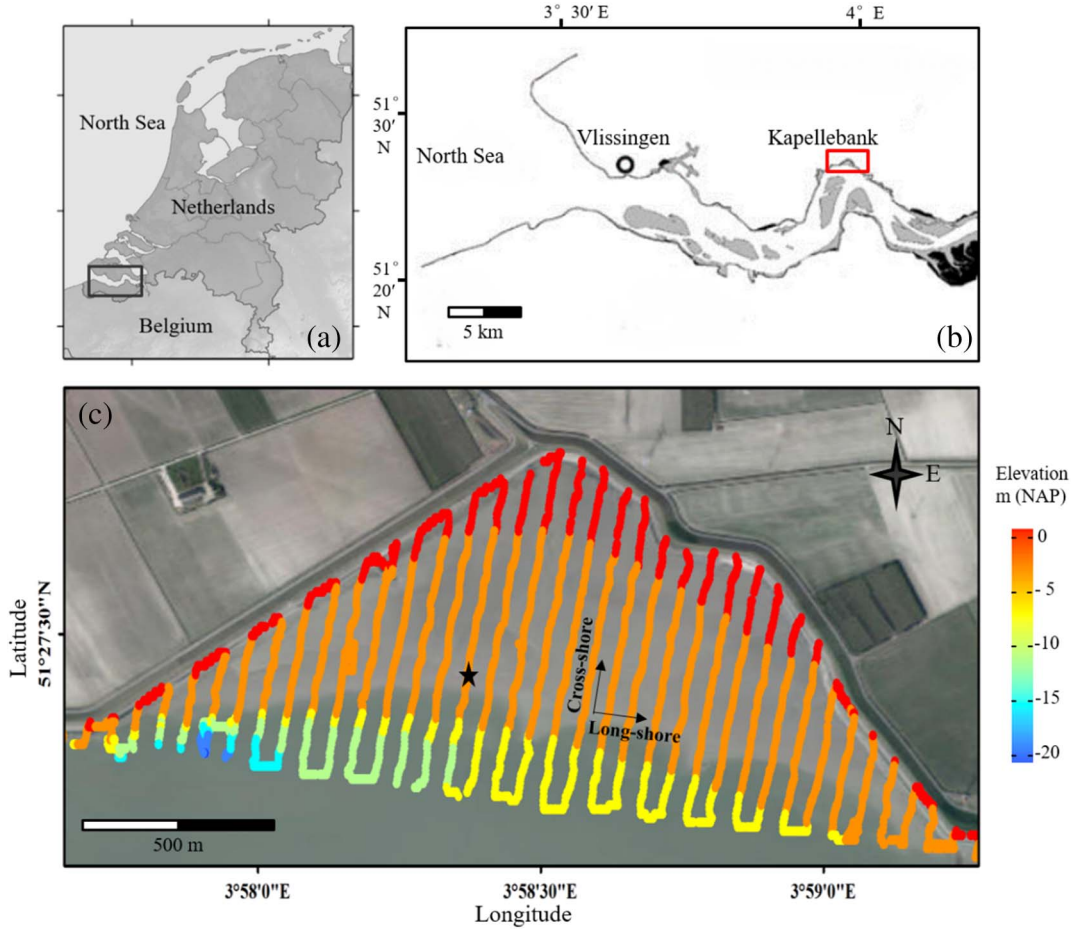

Fig. 1. (a) Geographic position of the lower Scheldt; (b) Location of the Kapellebank tidal flat; (c) The bathymetry of Kapellebank and the field observation site (marked as black star). NAP is about mean sea level.

(Verney et al., 2007). To ensure the reliability of ADV-derived data, raw velocity fluctuations were processed by removing all results with signal-to-noise (SNR) < 5 dB, and correlation < 70% as suggested by Chanson et al. (2008). The energy spectral analysis was then used to separate the turbulent kinetic energy of current-induced ($u_c'^2$, $v_c'^2$, $w_c'^2$) and wave-induced ($u_w'^2$, $v_w'^2$, $w_w'^2$) variances, and the influence of wave was expected to be between 0.1 and 1 Hz (Soulsby and Humphery, 1990; Verney et al., 2007). The combined bed shear stress was obtained from shear stress due to currents τ_c and due to waves τ_w (Wiberg and Smith, 1983):

$$\tau_{cw} = \sqrt{\tau_c^2 + \tau_w^2} \tag{1}$$

Current-induced bed shear stress was determined by the modified TKE method which uses only the vertical velocity fluctuations (Kim et al., 2000):

$$\tau_c = 0.9\rho_w \overline{w_c'^2} \tag{2}$$

where ρ_w is the water density (1030 kg m^{-3}). This relationship requires the measurements be taken within the constant stress layer. As this study was conducted on an intertidal mudflat, the ADV measurement volume may have been above this layer in very shallow water at times, but we consider it a minor influence at this close to bed height (15 cm). Wave shear stress is estimated by (Hansen and Reidenbach, 2012):

$$\tau_w = 0.5 f_w \rho_w U_w^2 \text{ with } f_w = 0.04\left(\frac{U_w T}{2\pi k_b}\right)^{-0.25},\ U_w = 2\sqrt{u_w'^2 + v_w'^2} \tag{3}$$

where f_w is the wave friction factor; U_w is the significant wave orbital velocity; T is the significant wave period; and k_b is the roughness height of the bottom, which is defined as $2.5D_{50}$.

2.3.2. Sediment dynamics

The OBS sensor was calibrated post-deployment in the laboratory due to the difficulty of collecting water samples on the tidal flat during the observation. Water samples used for calibration were obtained at the high concentration fringe at the water line under low wave condition, thus the calibration was representative of fine-grained suspended sediment. The correlation coefficient R^2 of the laboratory calibration was 0.95 (data point N = 26, figure not shown).

The LISST data have been checked before further processing, and low quality data with optical transmission < 15% were neglected (recommended by the manufacturer). These low quality data were mainly due to the occurrence of high SSC (> 0.8 g l^{-1}). Mean floc size D_M was obtained from the volume concentration distribution measured by the LISST. The floc effective density $\Delta\rho$ (i.e., bulk density less the water density) was determined by using results of the LISST and OBS, following Mikkelsen and Pejrup (2001):

$$\Delta\rho = \rho_f - \rho_w = \frac{M_f}{V_f} - \rho_w = \left(1 - \frac{\rho_w}{\rho_p}\right)\frac{M_p}{V_f} \tag{4}$$

where ρ_f is floc density, ρ_p is the primary particle density which is estimated to be about 2500 kg m^{-3}, given a density of 2650 and 1300 kg m^{-3} for mineral particulates and organic matter, respectively (Markussen and Andersen, 2013), and an organic matter content of 9% (mass ratio) determined by loss on ignition. M_f is the floc mass per unit volume, V_f indicates the floc volume concentration observed by LISST, and M_p is the SSC derived from calibrated OBS-3 + results.

The settling velocity of floc ω_s was estimated by using Stokes' Law. When the particle Reynolds number $\mathrm{Re} = \omega_s D_M \rho_w/\mu > 1$, indicating flocs fell beyond the viscous Reynolds region, a modified formula was applied to account for inertial drag during floc's settling (Winterwerp, 1998):

$$\omega_s = \frac{\Delta \rho g D_M^2}{18\mu} \text{ for } \mathrm{Re} = \omega_s D_M \rho_w/\mu < 1.$$

$$\omega_s = \frac{\alpha}{18\beta}\frac{\Delta \rho g D_M^2}{\mu(1 + 0.15Re^{0.687})} \text{ for } Re = \omega_s D_M \rho_w/\mu > 1 \quad (5)$$

where g is the acceleration due to gravity (9.8 m s^{-2}), μ is the molecular viscosity of water (t = 14 °C, $\mu = 1.17 \times 10^{-3}$ Pa s). α and β are coefficients depending on the shape of particles. In this study, flocs were considered to be spherical particles with $\alpha = 1$ and $\beta = 1$.

The topmost bed sediment (~1 cm thick layer) collected on April 29 was analyzed using a Mastersizer 2000 (measuring range 0.02–2000 μm, reproducibility error < 3%) after H_2O_2 and sodium metaphosphate treatment to remove organic matter and disaggregate flocs, respectively, and 15 min of sonification. Results showed that the median and mean grain size of the bed samples were 48.7 and 30.7 μm, respectively, constituting of about 13% clay (< 4 μm), 46% silt (4–62 μm), 30% very fine sand (62–125 μm), and 11% fine sand (125–250 μm). Organic matter content of the bed sediment was determined through ignition at 450 °C for 6 h, and results showed that organic matter content of the surface bed sediment was about 9% (± 1%).

3. Results

3.1. General time series

Time series of 25 days' hydrodynamics and SSC over the mudflat during tidal immersion are shown in Fig. 2. A storm was observed during the measurement period, i.e., the grey part between May 6 and 12. During stormy conditions, the mean wind speed was 12.0 m s^{-1}, and wind directions were mainly in northeastward direction, i.e., from the main channel towards the flat (Fig. 2a). Wind speeds were much smaller during calm conditions, with a mean value of 3.6 m s^{-1}. The significant wave height *Hs* was typically < 0.1 m during calm weather, and increased significantly during the storm, reaching up to 0.5 m on May 10 (Fig. 2b).

Fig. 2c shows the variation of water depth with a strong semi-diurnal signal. The measurement period started during spring tides with a maximum water depth of approximately 4.5 m. Note that the storm occurred between neap tide (May 6–8) to middle tide, with the maximum water depth of about 3.8 m to 4.1 m. Variations of long- and cross-shore flow velocities at 15 cmab (u and v, respectively) are presented in Fig. 2d. Flood currents (positive u) were overall stronger than ebb currents (negative u). The maximum flood and ebb velocities were about 0.4 and 0.3 m s^{-1}, respectively. Cross-shore currents (v) mainly occurred in the off-shore direction during the ebb tides and were typically < 0.1 m s^{-1}. During the storm (May 6–12), long-shore current velocities (u) were influenced by increased wind speed: the eastward currents (positive u) were observed for most of the time within tidal cycles. Off-shore currents more regularly occurred and lasted longer time around low water (LW) during the stormy conditions than those during calm conditions. The maximum off-shore currents up to ~0.2 m s^{-1} were observed between May 10–11.

Variations of current-induced shear stress τ_c, wave-induced τ_w, and the total shear stress τ_{cw} are presented in Fig. 2e. During calm weather, wave-induced shear stress was mainly below 0.02 N m^{-2}, and the maximum current-induced shear stress was about 0.3 N m^{-2}. Both τ_c and τ_w increased significantly during the stormy weather with the maximum values reaching 1.2 and 1.0 N m^{-2}, respectively. The shear stress during storm approaches better the diurnal tidal signal while during calm periods it corresponds better with a quarter-diurnal signal. It should be noted that as significant erosion occurred during the storm, the shear stresses might be underestimated a little in the end of the storm period compared to those in the beginning of the measurement due to the increase of distance between ADV sensor and bed surface.

Fig. 2f shows that SSC changed in a wide range between 0.01 and 4.0 g l^{-1} during this survey. Note that the maximum SSC before the storm (April 28 to May 6) was smaller than that after the storm, with nominal values of ~1.5 and 3.5 g l^{-1} for these two calm periods, respectively. Variations in shear stress as well as SSC within the tidal cycle under different weather conditions will be discussed later in Sections 3.3 and 3.4.

Fig. 2g shows the bed level variation reflecting the processes of erosion and deposition. Bed level remained stable during the calm conditions before the storm with ~3 mm net erosion (not clear in the figure due to the large scale) during spring tides between April 29 and May 2, and a deposition of ~7 mm in the following middle tides. During the storm, the bed eroded more quickly with bed level dropping incrementally at low waters and amounting to a net loss of ~110 mm over six days. The most significant erosion of ~50 mm occurred over two LW periods in two tidal cycles between May 10 and May 11. After the storm, a deposition of ~40 mm was measured in a week between May 15 and 22. Note that the ADV was reset and the initial bed elevation was plotted as zero on May 15. Contrary to erosion process during the storm, deposition process after the storm was quite smooth.

3.2. In situ particle size distributions (PSDs)

Time series of in situ floc size distributions are presented in Fig. 3a as volume fractions of 32 groups of particles ranging from 2.5 to 500 μm. The frequency of each size class is calculated by dividing the volume of each class by the total volume detected by the LISST. Two modes were observed in the PSDs, one was between ~80–200 μm, and the other was around 400 μm. Unlike the smaller mode, which could be found in nearly all the observation periods, the occurrence of the larger mode was not continuous but at regular intervals, related to flood-ebb tidal cycles. Fig. 3b shows the changes of mean floc size D_M and water depth. D_M ranged between ~50–200 μm, and exhibited strong intra-tidal variations in phase with water depth. The variation of D_M during the stormy periods was periodic, increasing with an increase in water depth, resulting in larger and smaller D_M at around high water (HW) and LW, respectively. During the calm periods, D_M was more irregular, while large flocs still occurred around HW.

3.3. Calm conditions pre- and post-storm

Fig. 4 shows typical data covering two tidal cycles (24 h) under pre- and post-storm periods, respectively. It was close to spring tide in April 28–29, with the maximum flood and ebb velocities values of ~0.42 and 0.32 m s^{-1}, respectively. The maximum flood and ebb velocities between May 19 and 20 were ~0.38 and 0.32 m s^{-1}, respectively. Current velocities were controlled by tidal dynamics, and it was flood dominated with larger peak flood velocities and longer flood durations than ebb tides. The maximum flood velocity occurred about an hour before HW, after that flood velocity dropped quickly and inversed to ebb currents within 2 h. Bed shear stress τ_{cw} varied between 0.01 and 0.25 N m^{-2} under these two calm conditions. At the beginning and end of tidal immersion, large SSC (> 0.5 g l^{-1}) were observed in shallow waters. The largest SSC in a tidal cycle was measured at about 1–2 h before HW, values were ~1.0 g l^{-1} before the storm and 2–3 times larger after the storm. The change of bed level was just within ~2–3 mm in a tidal cycle before the storm, with no clear erosion/deposition pattern. However, under the calm conditions after the storm, significant deposition of ~4–5 mm was observed around HW, following a slight erosion in the ebb tide, and about 3 mm of net deposition was left per tide.

Fig. 4d shows the variations of mean floc size D_M and floc effective

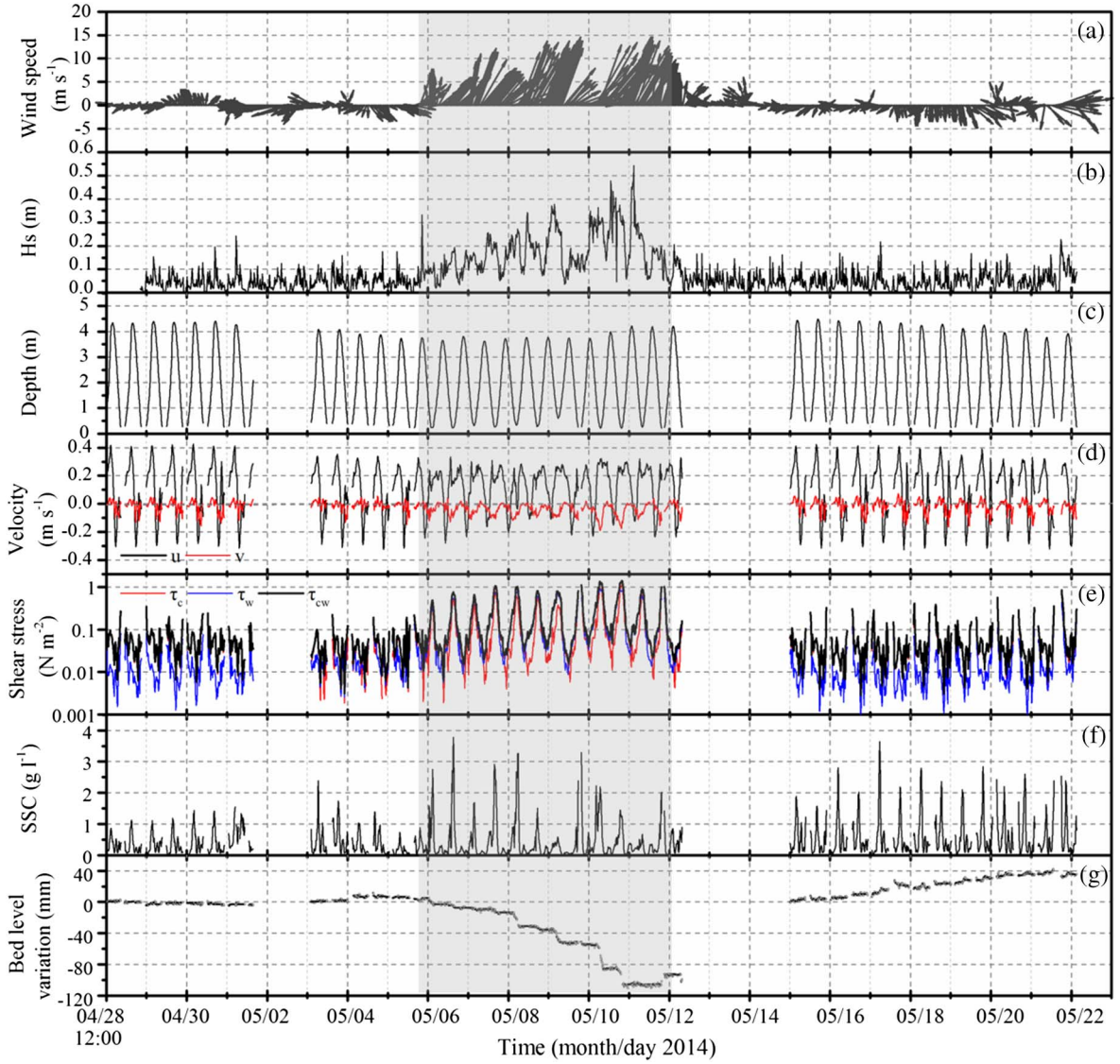

Fig. 2. Time variations of (a) wind speed and direction; (b) significant wave height *Hs*; (c) water depth; (d) long- and cross-shore flow velocity *u* and *v* at 15 cmab, respectively; (e) current-induced τ_c, wave-induced τ_w, and total shear stress τ_{cw}, respectively; (f) suspended sediment concentration (SSC) at 15 cmab; and (g) bed level variation. Negative value indicates bed erosion, and the bed level variation was reset on May 15. The grey shaded area between May 6 and May 12 covers the stormy periods.

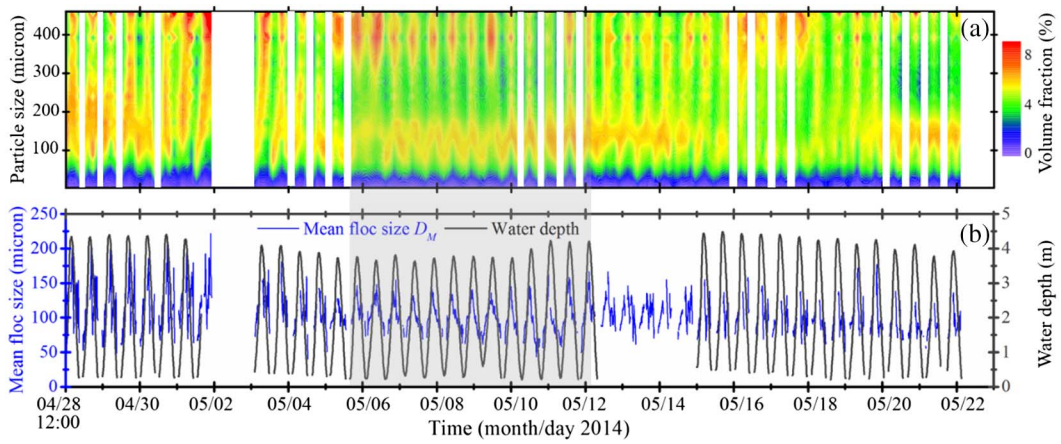

Fig. 3. Time evolution of (a) in situ floc size distribution, white columns cover periods without data around LW; (b) mean floc size D_M (blue line, the left y axis) and water depth (black line, the right y axis). The grey shaded area between May 6 and May 12 covers the storm period. (For interpretation of the references to colour in this figure legend, the reader is referred to the web version of this article.)

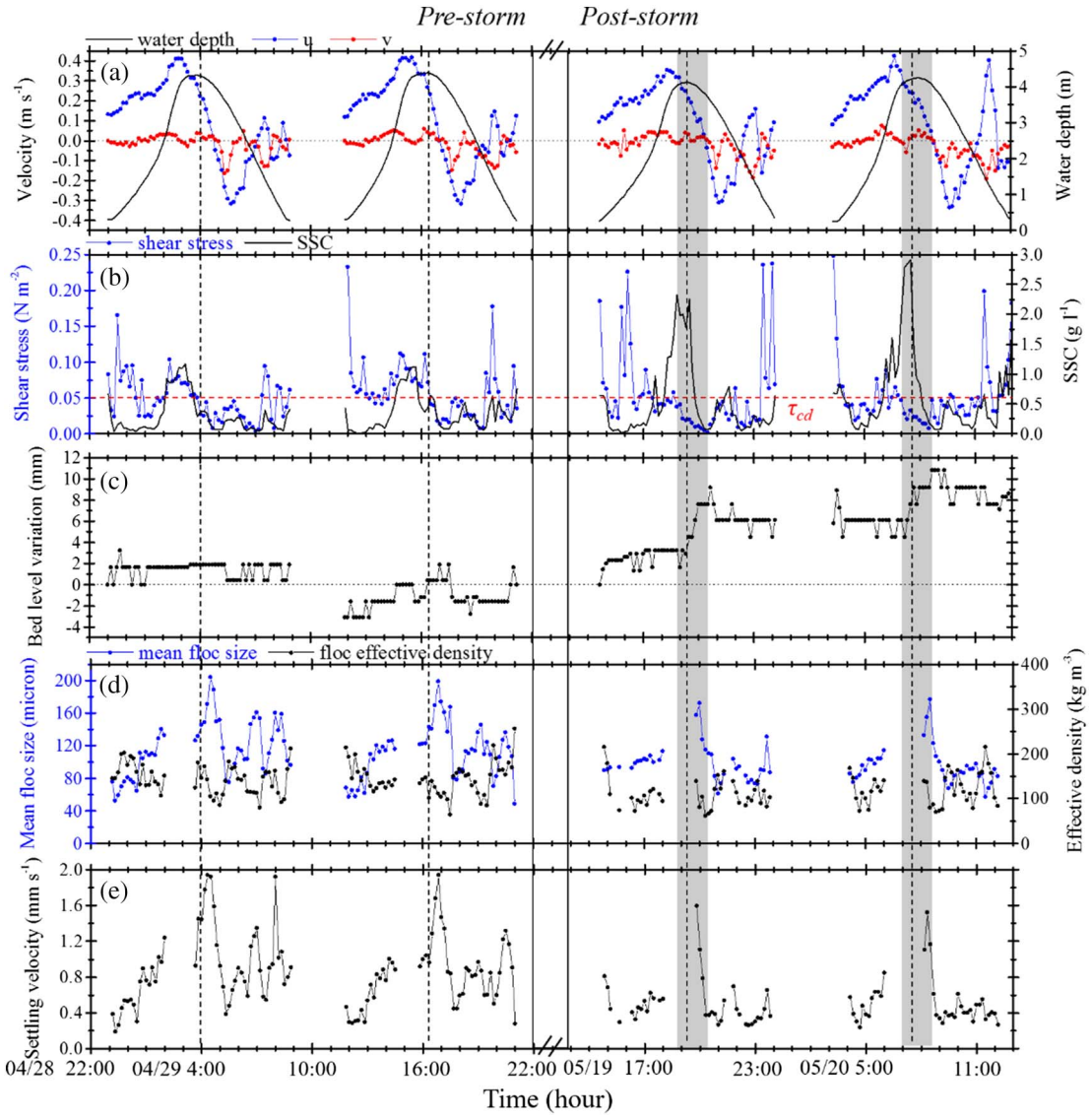

Fig. 4. Typical data under calm conditions pre- and post-storm on April 28–29 and May 19–20, respectively: (a) water depth (black line), long-shore velocity u (blue line), and cross-shore velocity v (red line); (b) bed shear stress τ_{cw} (blue line) and suspended sediment concentration SSC (black line), the red dash line indicates the value of critical shear stress for deposition τ_{cd}; (c) bed level variation; (d) mean floc size D_M (blue line) and floc effective density $\Delta\rho$ (black line); (e) floc settling velocity ω_s. The four vertical dash lines correspond to HW, and the grey shaded areas cover the major deposition processes. (For interpretation of the references to colour in this figure legend, the reader is referred to the web version of this article.)

density $\Delta\rho$, the gaps around HW were due to unreliable LISST results under high SSC. Floc size ranged from 50 to 200 μm before the storm, and the range decreased to 60–180 μm after the storm. The variation of D_M with tidal phase under these two calm periods was similar: D_M increased gradually from LW to HW and reached the peak value around HW slack, after that D_M decreased ~50% down to about 80 μm in 1 h. Then D_M fluctuated within 80–160 μm (pre-storm) and 80–120 μm (post-storm) over the next 4 h. $\Delta\rho$ changed between 60 and 250 kg m^{-3} within the tidal cycle, and smaller effective densities usually corresponded to larger mean floc sizes. Floc settling velocity ω_s, presented in Fig. 4e, varied between 0.2 and 2.0 mm s^{-1} and 0.2–1.6 mm s^{-1} before and after the storm, respectively, and followed a similar trend to D_M throughout a tidal cycle.

The typical in situ PSDs within a tidal cycle during the calm weather are presented in Fig. 5. The LISST derived sediment particle size distributions revealed varied unimodal and bimodal patterns at different tidal phases. It was found that in situ PSD in the beginning of the flood tide was similar to that of the bed sediment (Fig. 5a), with the mode being slightly coarser than the corresponding mode of the bed sediment (~80 μm). As flood ebb continued, the peak of in situ PSD shifted towards the coarser end, and another larger mode occurred when it came close to HW and around HWS (Fig. 5c and d). Soon after the HWS, the PSD became unimodal again and the peak shifted towards the finer end close to the peak of bed sediment, with the mean floc size decreased significantly from 189 to 77 μm. Then the peak of PSD shifted between the coarser and finer part as mean floc size fluctuated in the late ebb tide. Note that there were raised tails at the coarser end of some distribution curves, which was due to the presence of particles beyond the measurement range of LISST (< 500 μm). These particles with diameter > 500 μm were likely to cause under-estimation of D_M to some degree. The effects of raising tails are minor under conditions like Fig. 5b and f, as the dominant portion of particles has been detected (Voulgaris and Meyers, 2004), while special attention should be paid around HWS.

3.4. Stormy conditions

Fig. 6 presents typical stormy data from May 10 to 11 when the most significant erosion occurred. During this period, the average wind speed was 15.3 m s^{-1}, and the onshore wind directions changed

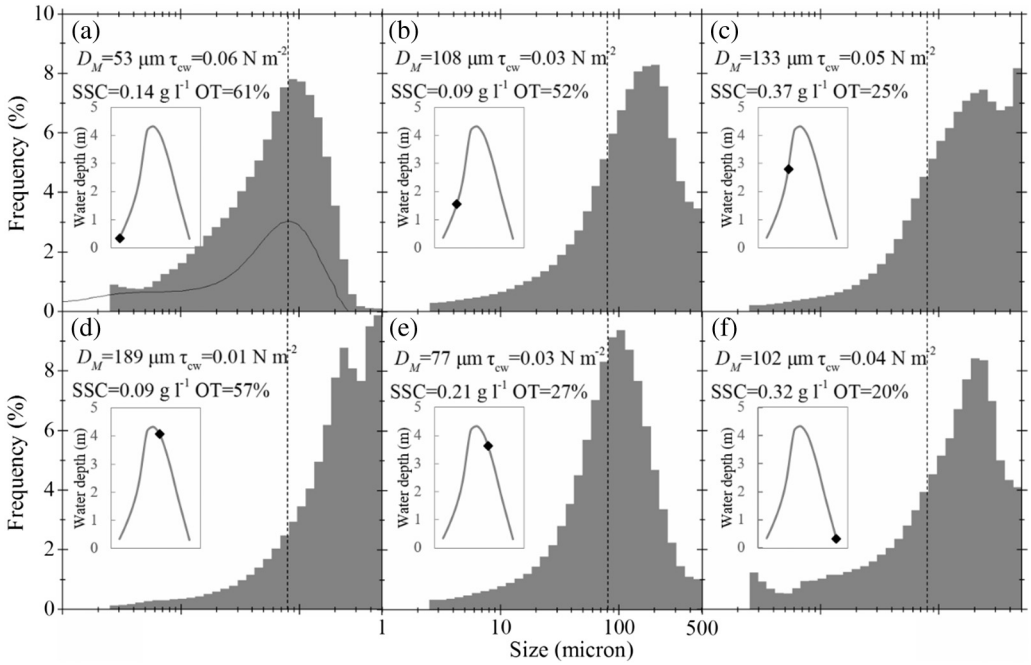

Fig. 5. Floc size distributions under different tidal phases during calm conditions on April 28–29. The black curve in (a) shows the dispersed grain size distribution of bed surface sediment, and the vertical dashed lines indicate the peak of the bed sediment distribution. OT indicates optical transmission over path of LISST.

between 230 and 250°. The wave activity was strong with the current velocity reaching ~0.35 m s^{-1} in shallow water and lasted until 2 h before HW. Off-shore currents (see red line in Fig. 6a) of ~0.1–0.2 m s^{-1} also continuously occurred in shallow water. The combined shear stress τ_{cw} ranged from about 0.04 to 1.5 N m^{-2}, an order of magnitude larger than for the calm conditions. The largest shear stress occurred around LW, and decreased rapidly to about 0.2 N m^{-2} when the water depth was more than ~1 m. During the stormy periods, SSC varied between 0.02 and 2.3 g l^{-1}, with the maximum value occurring around LW and a smaller peak of SSC (~0.5 g l^{-1}) was measured before HW in the tidal cycle. D_M increased from the minimum of 60 μm in shallow water to the maximum of 160 μm close to HW, and after that it decreased gradually with decreasing water depth. Relative large floc effective density over 200 kg m^{-3} was measured in shallow water, and Δρ decreased quickly to about 50 kg m^{-3} in the beginning of the flood phase. Floc settling velocity in the stormy conditions was between 0.2 and 1.2 mm s^{-1}, and the largest ω_s was found about 1–2 h before the HW.

Fig. 7 shows the in situ PSDs within a tidal cycle during the stormy weather. It was found that the variations of PSDs were quite asymmetrical between flood and ebb tide. The peak of PSD shifted towards the coarser end during flood tide, then reversed to the finer end during ebb tide. The PSD in the beginning of flood resembled that in the end of ebb tide, with similar peak corresponding to the mode of the bed sediment (Fig. 7a and f).

In summary, large differences have been found in the hydrodynamics and sediment dynamics in storm/calm conditions. During the stormy periods, positive long-shore currents lasted longer in a tidal cycle, and off-shore currents around LW were more significant than those in calm periods. The maximum SSC as well as bed erosion occurred around LW during the storm, however, the maximum SSC and bed deposition (post-storm) in a tidal cycle under the calm conditions were observed around HW. Mean floc size D_M showed an overall increase with the increase of water depth for both storm and calm conditions, and it decreased gradually from HW to LW during the storm, while D_M dropped quickly and was more fluctuate after reaching the maximum around HW during the calm conditions.

4. Discussions

4.1. Intra-tidal flocculation dynamics under different forcing conditions

Among many factors influencing flocculation, turbulence was expected to play the determining role in sediment flocculation in tidal cycles (Winterwerp, 1998; Dyer and Manning, 1999). Relationships between mean floc size D_M, shear stress τ_{cw} and concentration SSC are presented in Fig. 8a and c. The measurements were split depending on weather condition (calm versus storm) and tidal phase (flood versus ebb). Considering the sediment dynamics following a strong storm were not quite typical, only the data before the storm were used as the representative of calm weather condition. The regressions of four conditions (calm flood/ebb and stormy flood/ebb) all illustrate negative correlations between D_M and shear stress, with regression parameters R^2 = 0.42 and 0.36 for calm flood and ebb, respectively, and higher regression parameters of 0.71 and 0.65 were obtained for storm flood and ebb, respectively.

Although the pattern that floc size tended to decrease with the increase of shear stress were similar, a significant shift of the regression lines was found during flood and ebb phases under stormy period, indicating asymmetrical aggregation/break-up processes between flood and ebb tides. This asymmetry can be seen more clearly in Fig. 8d, which shows the typical variation of mean floc size within a tidal cycle. It can be interpreted from the asymmetry that floc sizes during flood are overall larger than those during ebb for the same shear stresses.

The asymmetrical flocculation behavior over the tide has been reported by a few authors and is attributed to the flocculation hysteresis effect, i.e. time scales for aggregation and break-up are different (e.g. Verney et al., 2011; Ramírez -Mendoza et al., 2016). In the laboratory research of Verney et al. (2011), they found that for a given shear rate, larger flocs were observed under increasing shear than those under decreasing shear, because the disruption of flocs was rapid once the shear force exceeded floc bond strength, while the aggregation process depended not only on moderate shear force, but also on collision efficiency and hence took longer time. However, the asymmetrical pattern observed in this case seemed to be contrary: flood tide (decreasing shear) showed larger flocs than ebb tide (increasing shear). This contrary result could be attributed to different environmental conditions under lab experiment and field survey. The same concentration of

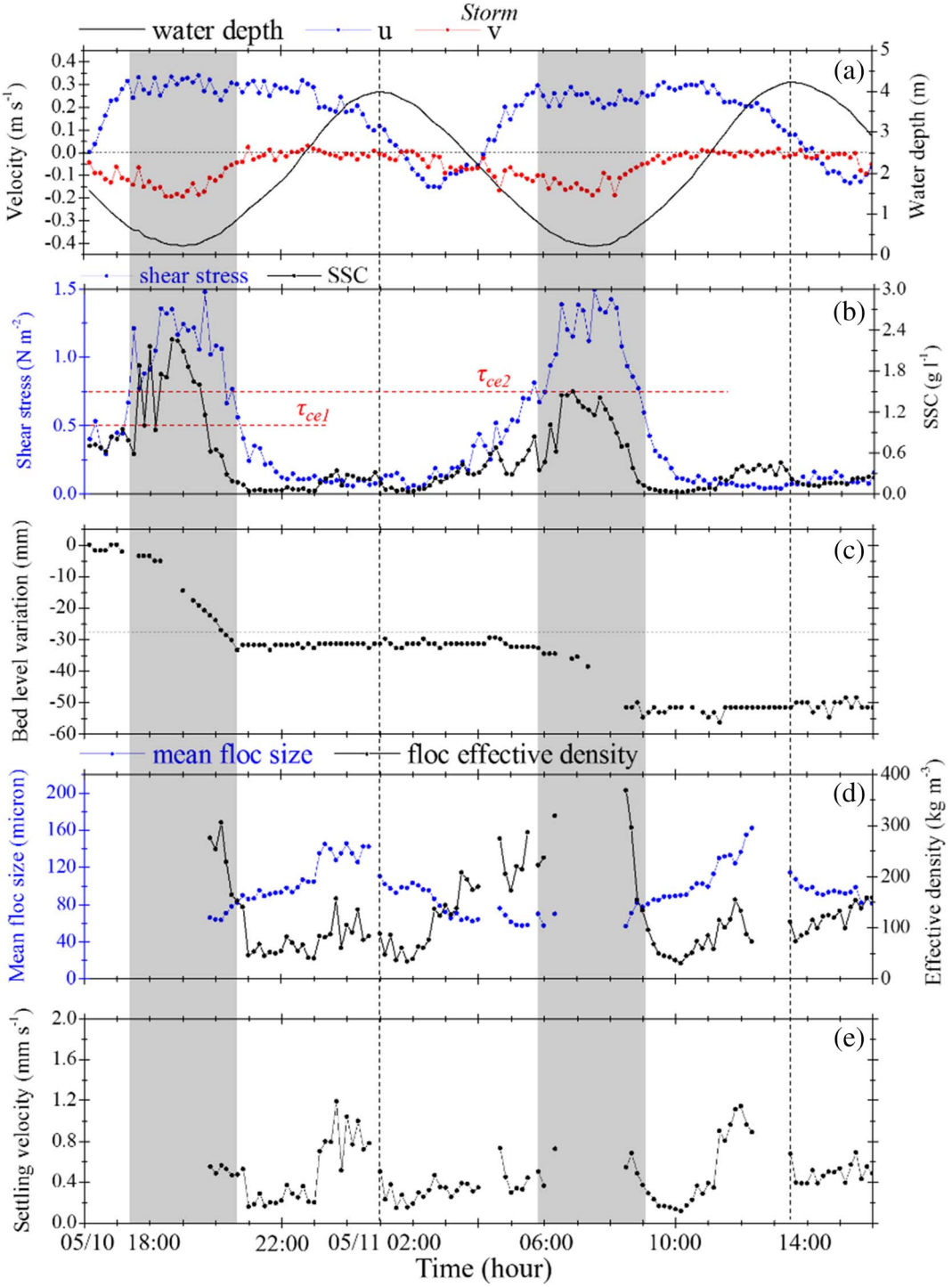

Fig. 6. Typical data under stormy conditions on May 10–11: (a) water depth (black line), long-shore velocity u (blue line), and cross-shore velocity v (red line); (b) bed shear stress τ_{cw} (blue line) and suspended sediment concentration SSC (black line), the red dash lines indicate the values of critical shear stresses for erosion: τ_{ce1} and τ_{ce2}; (c) bed level variation; (d) mean floc size D_M (blue line) and floc effective density $\Delta\rho$ (black line); (e) floc settling velocity ω_s. The two vertical dash lines correspond to HW, and the grey shaded areas cover the major erosion processes. (For interpretation of the references to colour in this figure legend, the reader is referred to the web version of this article.)

sediment was kept in suspension in the lab work of Verney et al. (2011), while significant resuspension (bed erosion) as well as settling took place during the storm in this study. As the bed sediment contains very fine (30%) and fine (11%) sand, the resuspension of bed sediment could change the constitutions of primary particles as well as sediment concentration thus affecting flocculation. The mixture of large-grain sand could also directly increase the particle size in suspension Meanwhile, Manning et al. (2010) found that sand could participate in flocculation and have important effects on the depositional behavior of mud/sand mixtures under the presence of natural biological adhesives. It was found that the modal peak of in situ PSD was significantly larger than that of bed sediment, except at low water when the shear stress was the strongest and erosion happened (Fig. 7), this may partially support the occurrence of mixed mud and sand flocculation.

The settling of larger flocs, especially around HWS, could be another reason for smaller floc size during ebb tide. Note that in the end of HWS, floc sizes dropped rapidly for both calm and stormy conditions (Fig. 8b and d), and this could explain the large gap between

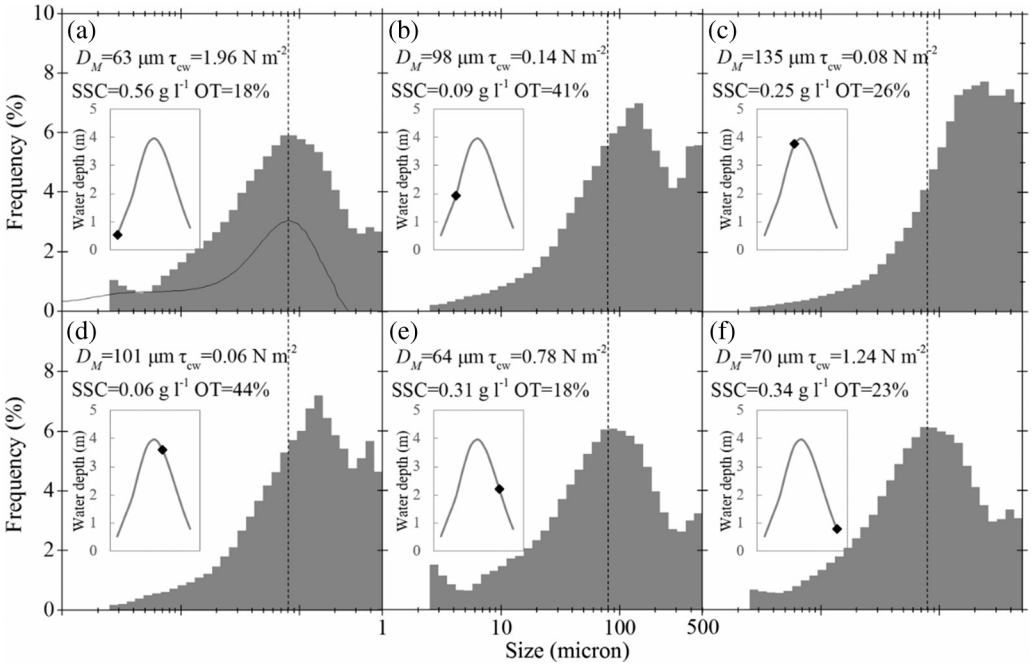

Fig. 7. Floc size distributions under different tidal phases during stormy conditions on May 10–11. The black curve in (a) shows the dispersed grain size distribution of bed surface sediment, and the vertical dashed lines indicate the peak of the bed sediment distribution. OT indicates optical transmission over path of LISST.

aggregation lines under low shear stress for calm conditions, although the asymmetry in the whole tidal cycle was not that clear. As mentioned before, floc sizes around HWS may be under-estimated to some degree due to the limited LISST measurement range, while the under-estimation in other tidal phases could be neglected, indicating that the decreasing of floc size after HWS might be more significant than that presented here.

According to the field survey, flood tide over the mudflat was characterized by a strong input of sediment, and large SSC in general, then settled around HW and was weekly resuspended during ebb tide.

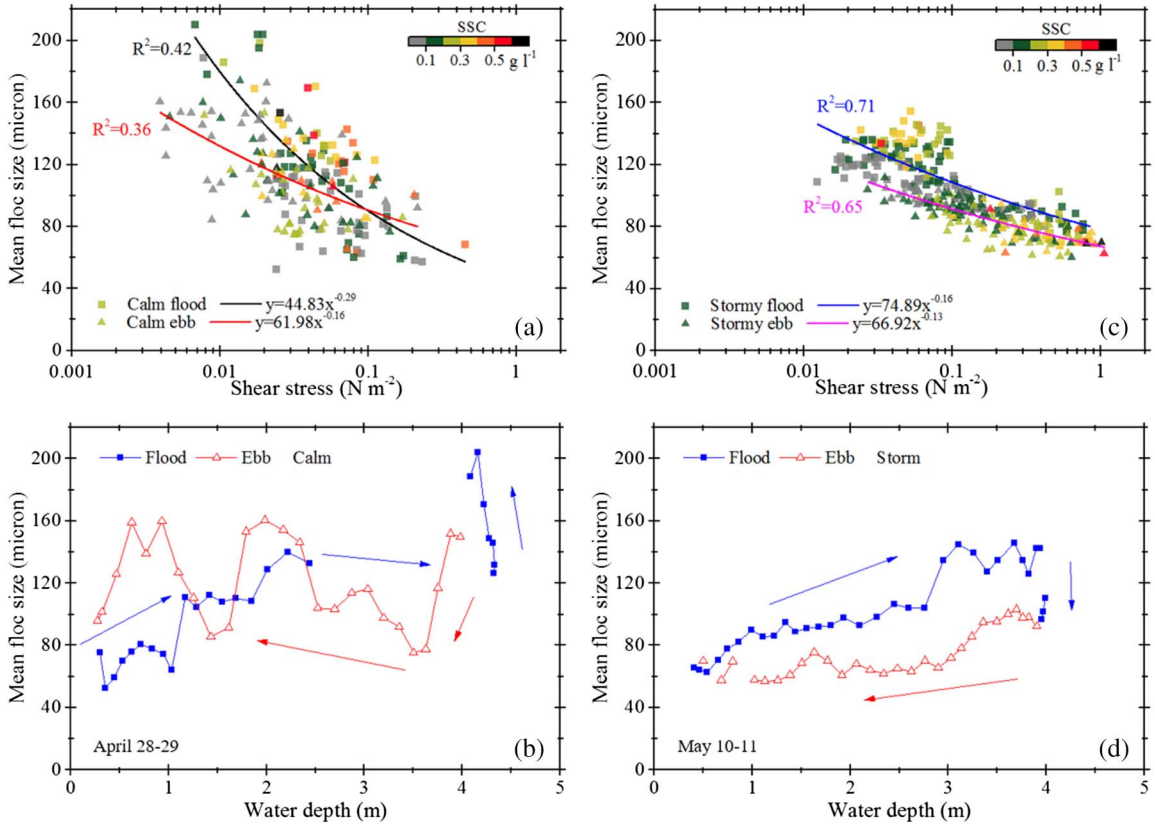

Fig. 8. (a)(c) Variation of mean floc size and shear stress under calm flood/ebb and stormy flood/ebb conditions, respectively; (b)(d) Typical variation of mean floc size with water depth in a tidal cycle under calm and stormy conditions on April 28–29 and May 10–11, respectively. In (a) and (c), solid lines are the regression results, and colour bar indicates corresponding suspended sediment concentration SSC. In (b) and (d), blue and red symbols represent flood and ebb tide, respectively. (For interpretation of the references to colour in this figure legend, the reader is referred to the web version of this article.)

Differences of SSC between flood and ebb tides emphasized the effect of concentration on flocculation for similar turbulence levels. It was well illustrated in Fig. 8a and c that in the shear range of ~0.03–0.1 N m^{-2}, mean floc sizes were overall larger with higher SSC, indicating that higher SSC may favor floc aggregation due to increased collision frequency. We could also scale the driving factors through Fig. 8a and c: turbulence is the dominant one, next SSC can modulate and enhance flocculation when turbulence decreases down.

4.2. Variation of floc effective density

Unlike the settling of non-cohesive sediment, the settling velocity of flocs not only relies on the particle size, but also on the floc structure, since the floc effective density is variable and related to the aggregation and break-up processes. Based on the self-similar fractal entities, Kranenburg (1994) proposed that: $\Delta\rho \propto (\rho_p - \rho_w)(D_M/d)^{N_f} - 3$, where d is the diameter of the primary particle and N_f is the floc fractal dimension, a mathematical parameter used as an indicator of particle morphology. N_f usually varied from 1.4 to 2.2 for large fragile flocs and strong flocs, respectively (Winterwerp, 1998). In the equation of Kranenburg (1994), N_f is a constant value over the size range for a certain simulation. However, some studies have noticed and used a variable fractal dimension with floc size in their simulations (e.g. Khelifa and Hill, 2006; Maggi, 2007; Kumar et al., 2010). The work of Khelifa and Hill (2006) suggested a quasi self-similar concept that N_f equals 3 for primary particles and then decreases with floc size in a power law function: $N_f = 3(D_M/d)^{\beta}$, $\beta = [\log(F_c/3)]/[\log(D_{fc}/d)]$, where D_{fc} is a characteristic floc size, and F_c is the corresponding fractal dimension when floc size increases to D_{fc}.

Fig. 9 exhibits the correlation between floc effective density $\Delta\rho$ and mean floc size D_M. It presents an overall decrease of effective density as mean floc size increases with $R^2 = 0.34$ and 0.33 for calm and stormy conditions, respectively. However, it was found in the figure that floc effective density decreased more rapidly with mean floc size and resulted in lower effective density under stormy conditions than that under calm conditions. For the calm conditions, we found that applying the Kranenburg (1994) equation with $N_f = 2$ and $d = 10$ μm was acceptable compared to the regression result, and it behaved better than the best fit using the Khelifa and Hill (2006) method. These results indicate that the floc fractal dimension may not be quite variable under calm conditions.

For the stormy conditions, however, neither the Kranenburg (1994) equation nor the Khelifa and Hill (2006) method could correctly simulate the observed dynamics. It was noted that ~16% of the points measured during the stormy conditions disagreed with the trend that effective density decreased with mean floc size and even showed a positive correlation between them. These points were measured in the late flood tide under mid to HW depth (> 2.5 m) when the turbulence was weak (< 0.1 N m^{-2}), and flocs were large with mean floc sizes over 100 μm. From the simulation results in Fig. 9b, it can be seen that variations of effective density with floc size are sensitive to both characteristic fractal dimension F_c and primary particle size d, however they are usually defined as constant values in the simulations for simplification, and this may explain why the reverse regime cannot be reproduced. During the storm, bed sediment as well as organic matter were resuspended at low waters when erosions happened, leading to the change of floc constitutions and could alter floc properties. With the anticipation of more organic matter in the aggregation and break-up processes, floc effective densities could be expected to be lower for the same mean floc sizes and flocs more resilient to shear breaking (Mietta et al., 2009), moreover, the fractal dimension of floc may also become more variable. Note that an OBS sensor was less sensitive for sand, thus OBS-derived SSC may be underestimated during the stormy condition, especially around LW when the most significant erosion occurred and bed sand resuspended. Therefore, the estimated floc effective density would be overall underestimated to some degree as well, however, this overall underestimation would not have great effect on the tendency of the variation of floc effective density with floc size.

By using variable characteristic fractal dimension F_c and primary particle size d in the simulations, it was found that the reverse regime could be reproduced (Fig. 10). Although we are not sure about the detail processes in the field, we think the great variations of floc structure as well as primary particle property during stormy conditions may explain why the 'classic' fractal approach fails and why this inverse regime is not observed during calm conditions.

4.3. Erosion and deposition processes under stormy and calm conditions

A few researches on the mudflat have concluded that the net import of suspended sediment usually happened in the form of repeated small imports in tidal cycles under the relative calm conditions, however, the net export was generally event controlled, such as in periods of strong on-shore wind (e.g. Christie et al., 1999; Andersen and Pejrup, 2001).

In this study, it was found that bed erosion during the storm occurred only around LW, when the shear stresses were the maximum and the off-shore velocities were significant. According to the bed level variation, the critical shear stress τ_{ce} in the beginning of the storm was ~0.15 N m^{-2} (data not shown), and it increased to about 0.50 N m^{-2}

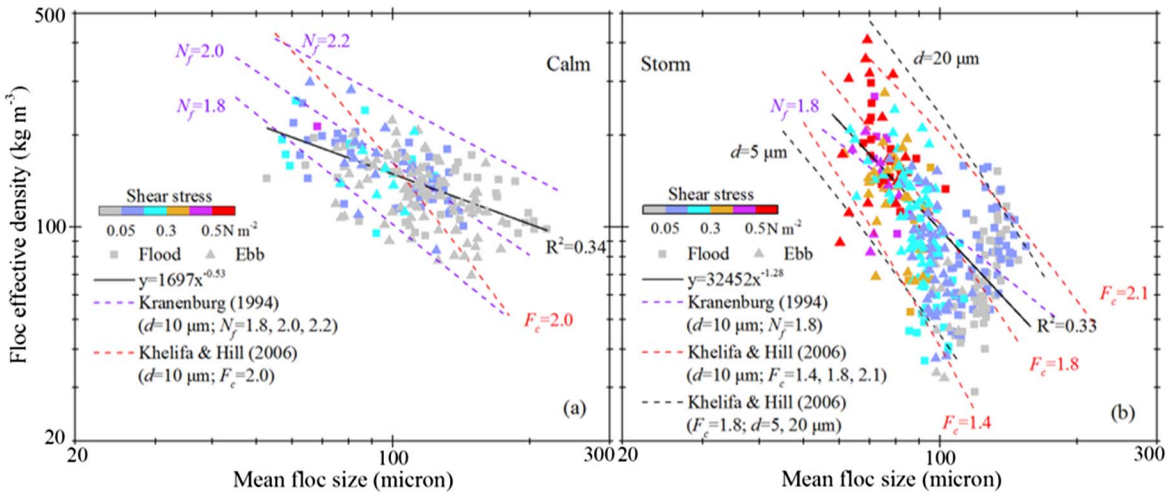

Fig. 9. Variation of floc effective density with mean floc size: (a) under calm conditions; (b) under stormy conditions. Solid black lines are the regression results, and dashed violet lines and dashed red (black) lines are results from the Kranenburg (1994) equation and the Khelifa and Hill (2006) method, respectively. D_{fc} = 100 μm in the simulations. Colour bar indicates corresponding shear stress. (For interpretation of the references to colour in this figure legend, the reader is referred to the web version of this article.)

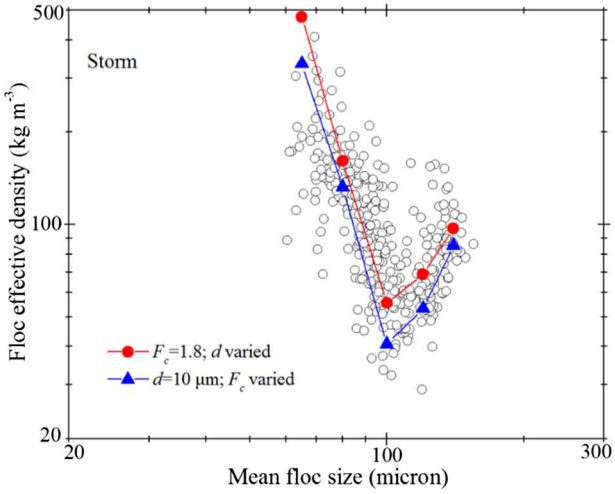

D_M (μm)	F_c	d (μm)	Δρ (kg m^{-3})
65	1.8	18	476.2
80	1.8	10	161.5
100	1.8	6	55.4
120	1.8	10	68.8
140	1.8	18	97.2
65	2	10	334.8
80	1.7	10	132.5
100	1.4	10	40.7
120	1.7	10	53.2
140	2	10	85.4

Fig. 10. Simulations of the variation of floc effective density with mean floc size in Khelifa and Hill (2006) method by using varied characteristic fractal dimension F_c and primary particle size d. D_{fc} = 100 μm in the simulations.

on May 10 after 60 mm erosion, τ_{ce} further increased to 0.75 N m^{-2} in the end of the erosion period after another 30 mm erosion (Fig. 6). Large amounts of sediment were resuspended due to the high shear stresses around LW, then probably transported towards the channel by the continuous off-shore currents before settling back to the bed. Thus off-shore velocity played a vital role in the advection of sediment away from the tidal flat (Christie et al., 1999; Le Hir et al., 2000).

In the calm conditions before the storm, the bed level was relatively stable with the shear stress below τ_{ce} (i.e. unable to erode the bed). A value of the critical shear stress for deposition τ_{cd} was estimated to be ~0.05 N m^{-2} based on the deposition processes that occurred after the storm (Fig. 4), meanwhile the values between 0.05 and 0.1 N m^{-2} were generally used in modelling studies (Whitehouse et al., 2000). The shear stress values before the storm were greater than τ_{cd} before HW when the maximum SSC occurred, and this could be the reason why deposition did not happen before the storm.

After the storm, smooth deposition processes lead to a 36% (40 mm/110 mm) recovery in a week. This kind of quick recovery after a storm has also been reported by some authors (e.g. Christie et al., 1999; Andersen and Pejrup, 2001). In the research of Andersen and Pejrup (2001), they found that an equivalent of ~40% of the net annual deposition happened in five tidal cycles following a storm. As for the exact deposition periods during the tidal cycle, we found that they were not fixed, with some occurring during HW and others between two tides (Fig. 11). Statistics show that about 15 mm (~2–5 mm each time) of deposition occurred at low waters between May 16 and 19 just after the spring tide, accounting for 37.5% of the total deposition. The reasons for these depositions were not clear for now because of a lack of data in shallow waters, we could not explain why they only happened at four low waters, neither. The remaining deposition events were all measured around HW when the maximum SSC were observed. The occurrence of high SSC (> 1.0 g l^{-1}) around HW was attributed to tidal advection and the settling of sediment from the upper water column, as the variation of bed level showed no correlation with resuspension (Fig. 4b and c). Moreover, it was found that SSC around HW after the storm were about twice the values before the storm. This increase was expected because the nearby waters became more turbid after importing of large amount of sediment eroded from the tidal flat. The floc settling velocity within this period was estimated to be as high as 1.6 mm s^{-1}, suggesting that only 47 min was required to settle over the full water depth of 4.5 m.

Deposition rate was estimated in two methods: (1) multiplying SSC and settling velocity of flocs; (2) multiplying bed level variation rate and sediment dry density (ρ_{dry} = 800 kg m^{-3}, assuming the water content of 90%). Time series of hourly averaged deposition rates estimated from these two approaches are presented in Fig. 11. Their results

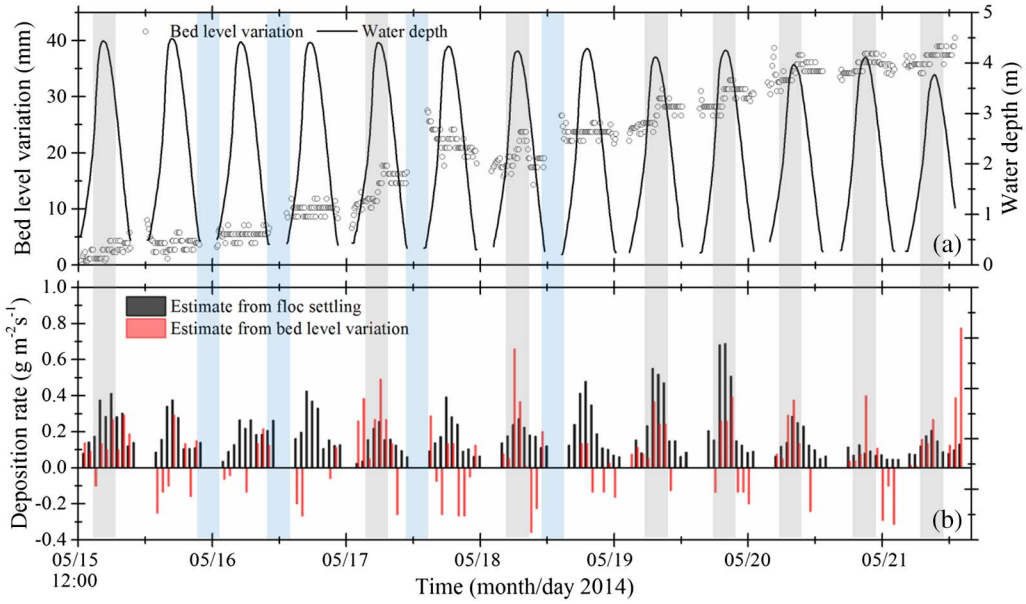

Fig. 11. Time series of (a) water depth and bed level variation; (b) deposition rate estimated from floc settling and bed level variation. The blue shaded areas cover bed accretion at low water, and the grey shaded areas cover bed accretion around high water. (For interpretation of the references to colour in this figure legend, the reader is referred to the web version of this article.)

were in the same order of magnitude, with the maximum value of about 0.7 $g\,m^{-2}\,s^{-1}$. Large deposition rate ($> 0.2\,g\,m^{-2}\,s^{-1}$) usually occurred around HW, and the estimated deposition rate from floc settling around HW matched with the deposition rate estimated from bed level variation. However, in the early flood and the late ebb tides, these two results were quite different: floc settling flux was about 0.1 $g\,m^{-2}\,s^{-1}$, while the bed level variation was often close to 0 or even negative for a short time, indicating that deposition did not actually happened, which may be because the shear stresses were larger than τ_{cd} in these periods.

5. Conclusions

Variations of floc characteristics in tidal cycles and the effects of shear stress and SSC on aggregation and break-up processes were investigated under stormy and calm weather conditions over a muddy tidal flat.

Mean floc size changed between ~50–200 μm and exhibited strong temporal variations within a tidal cycle. Negative relationships between mean floc size and bed shear stress were found under both calm and stormy conditions, and asymmetries between flood and ebb phases were identified. This asymmetrical behavior was likely due to significant resuspension and settling processes in the field, and resulted in an overall larger mean floc size during the flood than during the ebb tide under the same shear stresses. Floc effective density showed an overall decrease with the increase of mean floc size, and two methods were used to simulate the correlation between them and were compared with the regression results. The simulation result with the Kranenburg (1994) equation by using a constant fractal dimension of 2 was acceptable during the calm conditions. While during the stormy conditions, a reverse regime of floc effective density increased with the increase of floc size was identified, when the floc size was larger than ~100 μm. This was likely due to the anticipation of resuspended bed sediment as well as organic matter in flocculation, and the observed dynamics could be reproduced by using variable characteristic fractal dimension or variable primary particle size in the Khelifa and Hill (2006) simulations.

Bed erosion during the storm only occurred around LW in a tidal cycle when the combined current-wave shear stress was maximum, and off-shore current played a significant role in the erosion process through transporting the resuspended sediment towards the channel within a short time. After the storm, about 40% of the erosion recovered within just one week, the fast settling of large flocs around HW plays significant role on the deposition process, resulting in ~60% of the total recovery.

Acknowledgements

This research is the joint-program between SKLEC (State Key Lab of Estuarine and Coastal Research, China) and TU Delft (the Netherlands). The authors wish to thank Xianye Wang, Qin Zhu and staffs from TU Delft, Rijkswaterstaat, NIOZ, UNESCO-IHE, and Deltares who participated in the field survey. Financial support was provided by the Natural Science Foundation of China (No. 51320105005, 41276080, 41506105), National Science and Technology Support Program (2013BAB12B05/02), China Post-Doc Fund (No. 2015M580306, 2016T90351), and the NWO-JSTP program (No. 542.00.007h). Professor Manning's contribution to this manuscript was partly funded by HR Wallingford Company Research project 'FineScale - Dynamics of Fine-grained Cohesive Sediment at Varying Spatial and Temporal Scales' (DDY0523). Great thanks to the anonymous reviewer and reviewer Dr. Romaric Verney, who have given substantive and really constructive comments and suggestions to the authors.

References

Agrawal, Y.C., Pottsmith, H.C., 2000. Instruments for particle size and settling velocity observations in sediment transport. Mar. Geol. 168, 89–114. http://dx.doi.org/10.1016/S0025-3227(00)00044-X.

Andersen, T.J., 2001. Seasonal variation in erodibility of two temperate, microtidal mudflats. Estuar. Coast. Shelf Sci. 53, 1–12. http://dx.doi.org/10.1006/ecss.2001.0790.

Andersen, T.J., Pejrup, M., 2001. Suspended sediment transport on a temperate, microtidal mudflat, the Danish Wadden Sea. Mar. Geol. 173, 69–85.

Chanson, H., Trevethan, M., Aoki, S., 2008. Acoustic Doppler velocimetry (ADV) in small estuary: field experience and signal post-processing. Flow Meas. Instrum. 19, 307–313. http://dx.doi.org/10.1016/j.flowmeasinst.2008.03.003.

Chen, M.S., Wartel, S., van Eck, B., van Maldegem, D., 2005a. Suspended matter in the Scheldt estuary. Hydrobiologia 540, 79–104.

Chen, M.S., Wartel, S., Temmerman, S., 2005b. Seasonal variation of floc characteristics on tidal flats, the Scheldt estuary. Hydrobiologia 540, 181–195. http://dx.doi.org/10.1007/s10750-004-7143-6.

Christiansen, T., Wiberg, P.L., Milligan, T.G., 2000. Flow and sediment transport on a tidal salt marsh surface. Estuar. Coast. Shelf Sci. 50, 315–331. http://dx.doi.org/10.1006/ecss.2000.0548.

Christie, M.C., Dyer, K.R., 1998. Measurements of the turbid tidal edge over the Skeffling mudflats. Geol. Soc. Lond. Spec. Publ. 139, 45–55. http://dx.doi.org/10.1144/GSL.SP.1998.139.01.04.

Christie, M.C., Dyer, K.R., Turner, P., 1999. Sediment flux and bed level measurements from a macro tidal mudflat. Estuar. Coast. Shelf Sci. 49, 667–688. http://dx.doi.org/10.1006/ecss.1999.0525.

Deloffre, J., Lafite, R., Lesueur, P., Verney, R., Lesourd, S., Cuvilliez, A., Taylor, J., 2006. Controlling factors of rhythmic sedimentation processes on an intertidal estuarine mudflat—role of the turbidity maximum in the macrotidal Seine estuary, France. Mar. Geol. 235, 151–164.

Droppo, I.G., Ongley, E.D., 1994. Flocculation of suspended sediment in rivers of southeastern Canada. Water Res. 28, 1799–1809. http://dx.doi.org/10.1016/0043-1354(94)90253-4.

Dyer, K.R., 1989. Sediment processes in estuaries: future research requirements. J. Geophys. Res. 94, 14327–14339. http://dx.doi.org/10.1029/JC094iC10p14327.

Dyer, K.R., 1998. The typology of intertidal mudflats. Geol. Soc. Lond. Spec. Publ. 139, 11–24.

Dyer, K.R., Manning, A.J., 1999. Observation of the size, settling velocity and effective density of flocs, and their fractal dimensions. J. Sea Res. 41, 87–95.

Fennessy, M.J., Dyer, K.R., Huntley, D.A., 1994. Inssev: an instrument to measure the size and settling velocity of flocs in situ. Mar. Geol. 117, 107–117. http://dx.doi.org/10.1016/0025-3227(94)90009-4.

Fettweis, M., Baeye, M., Zande, D., van der Eynde, D., van der Lee, B.J., 2014. Seasonality of floc strength in the southern North Sea. J. Geophys. Res. Oceans 119, 1911–1926. http://dx.doi.org/10.1002/2013JC009750.

Fugate, D.C., Friedrichs, C.T., 2003. Controls on suspended aggregate size in partially mixed estuaries. Estuar. Coast. Shelf Sci. 58, 389–404. http://dx.doi.org/10.1016/S0272-7714(03)00107-0.

Gartner, J.W., Cheng, R.T., Wang, P.F., Richter, K., 2001. Laboratory and field evaluations of the LISST-100 instrument for suspended particle size determinations. Mar. Geol. 175, 199–219. http://dx.doi.org/10.1016/S0025-3227(01)00137-2.

Guo, L., He, Q., 2011. Freshwater flocculation of suspended sediments in the Yangtze River, China. Ocean Dyn. 61, 371–386.

Hansen, J.C.R., Reidenbach, M.A., 2012. Wave and tidally driven flows in eelgrass beds and their effect on sediment suspension. Mar. Ecol. Prog. Ser. 448, 271–287. http://dx.doi.org/10.3354/meps09225.

Hill, P.S., Newgard, J.P., Law, B.A., Milligan, T.G., 2013. Flocculation on a muddy intertidal flat in Willapa Bay, Washington, part II: observations of suspended particle size in a secondary channel and adjacent flat. Cont. Shelf Res. 60, S145–S156. http://dx.doi.org/10.1016/j.csr.2012.06.006.

Khelifa, A., Hill, P.S., 2006. Models for effective density and settling velocity of flocs. J. Hydraul. Res. 44, 390–401. http://dx.doi.org/10.1080/00221686.2006.9521690.

Kim, S.C., Friedrichs, C.T., Maa, J.P.Y., Wright, L.D., 2000. Estimating bottom stress in tidal boundary layer from acoustic Doppler velocimeter data. J. Hydraul. Eng. 126, 399–406.

Kranck, K., Milligan, T.G., 1992. Characteristics of suspended particles at an 11-hour anchor station in San Francisco Bay, California. J. Geophys. Res. Atmos. 971, 11373–11382.

Kranenburg, C., 1994. The fractal structure of cohesive sediment aggregates. Estuar. Coast. Shelf Sci. 39, 451–460. http://dx.doi.org/10.1016/S0272-7714(06)80002-8.

Kuijper, C., Steijn, R., Roelvink, D., 2004. Morphological Modelling of the Western Scheldt.

Kumar, R.G., Strom, K.B., Keyvani, A., 2010. Floc properties and settling velocity of San Jacinto estuary mud under variable shear and salinity conditions. Cont. Shelf Res. 30, 2067–2081. http://dx.doi.org/10.1016/j.csr.2010.10.006.

Law, B.A., Milligan, T.G., Hill, P.S., Newgard, J., Wheatcroft, R.A., Wiberg, P.L., 2013. Flocculation on a muddy intertidal flat in Willapa Bay, Washington, part I: a regional survey of the grain size of surficial sediments. Cont. Shelf Res. 60, S136–S144. http://dx.doi.org/10.1016/j.csr.2012.06.007.

Le Hir, P., Roberts, W., Cazaillet, O., Christie, M., Bassoullet, P., Bacher, C., 2000. Characterization of intertidal flat hydrodynamics. Cont. Shelf Res. 20, 1433–1459.

Maggi, F., 2007. Variable fractal dimension: a major control for floc structure and flocculation kinematics of suspended cohesive sediment. J. Geophys. Res. Oceans 112, 1–12. http://dx.doi.org/10.1029/2006JC003951.

Manning, A.J., Dyer, K.R., 1999. A laboratory examination of floc characteristics with regard to turbulent shearing. Mar. Geol. 160, 147–170. http://dx.doi.org/10.1016/S0025-3227(99)00013-4.

Manning, A.J., Dyer, K.R., 2007. Mass settling flux of fine sediments in northern European

estuaries: measurements and predictions. Mar. Geol. 245, 107–122. http://dx.doi.org/10.1016/j.margeo.2007.07.005.
Manning, A.J., Baugh, J.V., Spearman, J.R., Whitehouse, R.J.S., 2010. Flocculation settling characteristics of mud: sand mixtures. Ocean Dyn. 60, 237–253.
Markussen, T.N., Andersen, T.J., 2013. A simple method for calculating in situ floc settling velocities based on effective density functions. Mar. Geol. 344, 10–18. http://dx.doi.org/10.1016/j.margeo.2013.07.002.
Mehta, A.J., Manning, A.J., Khare, Y.P., 2014. A note on the krone deposition equation and significance of floc aggregation. Mar. Geol. 354, 34–39. http://dx.doi.org/10.1016/j.margeo.2014.04.002.
Mietta, F., Chassagne, C., Manning, A.J., Winterwerp, J.C., 2009. Influence of shear rate, organic matter content, pH and salinity on mud flocculation. Ocean Dyn. 59, 751–763. http://dx.doi.org/10.1007/s10236-009-0231-4.
Mikkelsen, O., Pejrup, M., 2001. The use of a LISST-100 laser particle sizer for in-situ estimates of floc size, density and settling velocity. Geo-Marine Lett. 20, 187–195.
Milligan, T.G., Hill, P.S., 1998. A laboratory assessment of the relative importance of turbulence, particle composition, and concentration in limiting maximal floc size and settling behaviour. J. Sea Res. 39, 227–241.
Milligan, T.G., Hill, P.S., Law, B.A., 2007. Flocculation and the loss of sediment from the Po River plume. Cont. Shelf Res. 27, 309–321. http://dx.doi.org/10.1016/j.csr.2006.11.008.
Ramírez -Mendoza, R., Souza, A.J., Amoudry, L.O., Plater, A.J., 2016. Effective energy controls on flocculation under various wave-current regimes. Mar. Geol. 382, 136–150. http://dx.doi.org/10.1016/j.margeo.2016.10.006.
Safak, I., Allison, M.A., Sheremet, A., 2013. Floc variability under changing turbulent stresses and sediment availability on a wave energetic muddy shelf. Cont. Shelf Res. 53, 1–10. http://dx.doi.org/10.1016/j.csr.2012.11.015.
Sahin, C., 2014. Investigation of the variability of floc sizes on the Louisiana Shelf using acoustic estimates of cohesive sediment properties. Mar. Geol. 353, 55–64.
Soulsby, R.L., Humphery, J.D., 1990. Field Observations of Wave-Current Interaction at the Sea Bed. Springer, Netherlands.
Soulsby, R.L., Manning, A.J., Spearman, J., Whitehouse, R.J.S., 2013. Settling velocity and mass settling flux of flocculated estuarine sediments. Mar. Geol. 339, 1–12. http://dx.doi.org/10.1016/j.margeo.2013.04.006.
Uncles, R.J., Bale, A.J., Brinsley, M.D., Frickers, P.E., Harris, C., Lewis, R.E., Pope, N.D., Staff, F.J., Stephens, J.A., Turley, C.M., Widdows, J., 2003. Intertidal mudflat properties, currents and sediment erosion in the partially mixed Tamar Estuary, UK. Ocean Dyn. 53, 239–251. http://dx.doi.org/10.1007/s10236-003-0047-6.
Verney, R., Deloffre, J., Brun-Cottan, J.C., Lafite, R., 2007. The effect of wave-induced turbulence on intertidal mudflats: impact of boat traffic and wind. Cont. Shelf Res. 27, 594–612. http://dx.doi.org/10.1016/j.csr.2006.10.005.
Verney, R., Lafite, R., Brun-Cottan, J.C., 2009. Flocculation potential of estuarine particles: the importance of environmental factors and of the spatial and seasonal variability of suspended particulate matter. Estuar. Coasts 32, 678–693. http://dx.doi.org/10.1007/s12237-009-9160-1.
Verney, R., Lafite, R., Brun-Cottan, J.C., Le Hir, P., 2011. Behaviour of a floc population during a tidal cycle: laboratory experiments and numerical modelling. Cont. Shelf Res. 31, S64–S83. http://dx.doi.org/10.1016/j.csr.2010.02.005.
Voulgaris, G., Meyers, S.T., 2004. Temporal variability of hydrodynamics, sediment concentration and sediment settling velocity in a tidal creek. Cont. Shelf Res. 24, 1659–1683. http://dx.doi.org/10.1016/j.csr.2004.05.006.
Whitehouse, R.J.S., Soulsby, R.L., Roberts, W., Mitchener, H.J., 2000. Dynamics of estuarine muds: a manual for practical applications. In: Report SR 527.
Wiberg, P., Smith, J.D., 1983. A comparison of field data and theoretical models for wave-current interactions at the bed on the continental shelf. Cont. Shelf Res. 2, 147–162.
Winterwerp, J.C., 1998. A simple model for turbulence induced flocculation of cohesive sediment. J. Hydraul. Res. 36, 309–326. http://dx.doi.org/10.1080/00221689809498621.
Winterwerp, J.C., Van Kesteren, W.G.M., 2004. Introduction to the Physics of Cohesive Sediment Dynamics in the Marine Environment. Elsevier.
Xia, X.M., Li, Y., Yang, H., Wu, C.Y., Sing, T.H., Pong, H.K., 2004. Observations on the size and settling velocity distributions of suspended sediment in the Pearl River estuary, China. Cont. Shelf Res. 24, 1809–1826. http://dx.doi.org/10.1016/j.csr.2004.06.009.